Available online at www.sciencedirect.com
SCIENCE DIRECT®
ELSEVIER
Nuclear Instruments and Methods in Physics Research A 554 (2005) 474–493
NUCLEAR INSTRUMENTS & METHODS IN PHYSICS RESEARCH Section A
www.elsevier.com/locate/nima

Modeling of ionization produced by fast charged particles in gases

I.B. Smirnov*

Petersburg Nuclear Physics Institute, Gatchina 188300, Russia

Received 1 August 2005; received in revised form 11 August 2005; accepted 16 August 2005
Available online 31 August 2005

Abstract

A computer modeling of ionization is necessary for the simulation of gaseous detectors of fast charged particles. The interactions of the incident particle with matter are well described by the photoabsorption ionization (PAI) model, which is based on the relation between the energy deposited by the fast charged particle in a medium and the photoabsorption cross-section of this medium. Some modification of the PAI model energy-transfer cross-section allows to distinguish the interactions with different atomic shells and to determine the energy of the primary photoelectrons and possible atomic relaxation cascades. Further simulation of paths and absorption of secondary particles results in a realistic reproduction of the space distributions and amount of initial ionization.

PACS: 34.50.Bw; 34.80.Dp; 29.40.Cs; 07.05.Tp

Keywords: Ionization; Modeling; Simulation; Gaseous detectors; PAI; Relaxation

1. Introduction

Detectors based on the registration of ionization produced by fast charged particles in gases are widely used in high-energy physics experiments. Their main role is the detection of the position of the track and the time of its passage without the particle being absorbed or any noticeable influence on its further movement being made. The amount of ionization deposited in the sensitive volume of the detector can also be measured and gives information about the particle charge and velocity. Despite the wide use of gas-filled detectors their computer modeling still represents a difficult problem. The large variety of phenomena and microscopic processes involved is difficult to simulate realistically in a detailed way or to reproduce reliably in a phenomenological way. The existing models are approximate and based on combining microscopic modeling of some

*Tel.: +7 813 7146912.
E-mail address: Igor.Smirnov@cern.ch.

0168-9002/$ - see front matter © 2005 Elsevier B.V. All rights reserved.
doi:10.1016/j.nima.2005.08.064

phenomena and well-established phenomenological or generalized features of the others.

When the incident particle passes through matter, it transfers a part of its energy to atoms through inelastic collisions with them. This energy is dissipated in matter by emission of a series of electrons and photons, which ionize other atoms and so on. The multiplication of liberated electrons ends when electron and photon energies become smaller than the minimal ionization potential of the matter. After that the liberated electrons remain free for some significant time. Together with ions, they may be called initial ionization. The modeling of their number and initial position is a goal of this research. We do not consider here what happens with the initial ionization later. Many important characteristics of the proportional chambers can be deduced just from the amount and space position of the initial ionization, while the other more detailed characteristics can be obtained after simulation of the other processes. The complete models, such as GARFIELD [1], can include the simulation of the drift of electrons and ions to chamber electrodes with various additional effects such as attachment, recombination, diffusion, fluorescence, avalanche amplification in the vicinity of the wires, space charge, charge induction at electrodes, influence of magnetic field. The complete simulation is a challenging problem. This paper is devoted to modeling the initial ionization only. It describes the model implemented in the latest version of the computer program HEED [2] developed in 2003–2005.[1] The abbreviation HEED stands for high-energy electrodynamics. The name was prompted by the title of the book "High Energy Electrodynamics in Matter" written by Akhiezer and Shulga [3] and indicates the relation between the ionization energy losses as well as Cherenkov and transition radiation (formerly also generated by one of the versions of this program) and the classical electrodynamic properties of media, crossed by high-energy particles. The former version of this program was used as a component of GARFIELD, and also together with other software packages in various important studies and developments [4–11]. The former version was written in Fortran-77, the new one is made in C++ and based on an improved physical model and arbitrary geometry. The new C++ version contains an interface package which allows it to be called from Fortran in approximately the same way as the old program. Calculations presented in this paper are made by the new C++ version.

There is a wide consensus that the rate of ionization processes occurring when a fast charged particle travels through a medium depends in a certain way on the cross-section of ionization of these atoms by real photons, and also on the dielectric permeability of this medium [12–22]. The dielectric permeability is a function of the photoabsorption cross-section of this medium. Following the work by Allison and Cobb [16] the corresponding theory is called the photoabsorption ionization (PAI) model. The model gives the cross-section of the energy transfers from the particle to the medium. At the practical application of this model for the description of the signals from gaseous detectors one usually assumes that the amount of ionization created after each energy transfer is approximately proportional to the transferred energy with some fluctuations. This approximation is usually sufficient for the practical calculations in which the little space scattering of ionization around the interaction point is not significant. Because of the small practical range of δ-electrons with an energy up to a few keV, and also because of the small probability of fluorescence, we can consider all the energy to be absorbed and converted into ionization at the point of interaction, except for chambers with a high position resolution or when investigating the processes that can depend on the density of the initial ionization (for example, the space-charge effect around anode wires of the proportional chamber). However, the ultimate spatial resolution of cathode strip and micropattern chambers (see, for example, Refs. [23,24]) is much smaller than the typical range of electrons of keV energies. The range of electrons and the fluorescent photon yield and range also play a role when studying the performance of transition radiation detectors and X-ray detectors.

[1]The program is currently available at http://cern.ch/ismirnov/heed.

In order to simulate the range of electrons and the fluorescent photons, one has to determine their energies. The energies of the emitted particles depend on the atomic shell that absorbs a portion of the transferred energy. Assuming that the transferred energy is absorbed by a single atomic electron, we conclude that the photoelectron should carry the transferred energy minus the binding energy of the given shell. Then the vacancy left by the knockout photoelectron can be filled with the emittance of fluorescence photons and secondary autoionization (Auger) electrons. The secondary electrons and photons are as a rule absorbed elsewhere, sometimes with emittance of new secondary products and so on. Since the original PAI cross-section gives the probabilities of interactions of the incident particle with the total atom, rather than with a single electron or a particular atomic shell, we have to modify or replace it by the cross-sections for individual shells. These partial cross-sections should, however, take into account the presence of the dielectric medium, in which all shells "participate" together. "Intuitive" separation based on deduction of the shell number from the transferred energy (choosing the shell with binding energy less than the transferred energy and nearest to it) is not always justified, in particular, in some gas mixtures and in wide gas layers. Although there are many research papers and computer programs devoted to or including the detailed calculation of ionization effects (starting from sixties of the last century see Refs. [12–22,25–36]), the full PAI model with separated shells and relaxation cascades for fast charged particles and arbitrary gas mixture has not been consistently developed and tested yet. The purpose of this work is to develop such a model and to test it. We will call it the photoabsorption ionization and relaxation (PAIR) model.

2. The model

2.1. Cross-section of energy transfers from incident particle to medium

The differential cross-section for the transfer of the energy E in a single collision of the incident particle with an atom, normalized per one atom of the absorbing media (see Ref. [16], and also Refs. [13–15,18–22]), is expressed by

$$\frac{\mathrm{d}\sigma}{\mathrm{d}E}=\frac{\alpha}{\beta^2\pi}\left(\frac{\sigma_\gamma(E)}{E}\ln\left(\frac{1}{\sqrt{(1-\beta^2\varepsilon_1)^2+\beta^4\varepsilon_2^2}}\right)+\frac{1}{N\hbar c}\left(\beta^2-\frac{\varepsilon_1}{|\varepsilon|^2}\right)\theta+\frac{\sigma_\gamma(E)}{E}\ln\frac{2m_\mathrm{e}c^2\beta^2}{E}+\frac{1}{E^2}\int_0^E\sigma_\gamma(E_1)\,\mathrm{d}E_1\right) \tag{1}$$

where m_e is the electron mass, βc is the velocity of the incident particle, $\alpha=1/137$ is the fine structure constant, $\sigma_\gamma(E)$ is the atomic photoabsorption cross-section for one atom, and N is the number of atoms per unit volume. Finally $\varepsilon=\varepsilon_1+\mathrm{i}\varepsilon_2$ and θ are the complex dielectric constant and angle calculated by

$$\varepsilon_1(E)=1+\frac{2}{\pi}P\int_0^\infty\frac{x\varepsilon_2(x)}{x^2-E^2}\,\mathrm{d}x,$$
$$\varepsilon_2(E)=\frac{N\hbar c}{E}\sigma_\gamma(E) \tag{2}$$

$$\theta=\arg(1-\varepsilon_1\beta^2+\mathrm{i}\varepsilon_2\beta^2)=\frac{\pi}{2}-\arctan\frac{1-\varepsilon_1\beta^2}{\varepsilon_2\beta^2} \tag{3}$$

P indicates that the principal value of the integral has to be taken.

The interpretation of the terms of Eq. (1) is given in Ref. [16]. In particular the last term represents the Rutherford scattering for those electrons that are quasi-free for an energy transfer E. Because of the Thomas–Reiche–Kuhn sum rule

$$\int_0^\infty\sigma_\gamma(E)\,\mathrm{d}E=\frac{2\pi^2\alpha Z}{m_e} \tag{4}$$

(where Z is the atomic number) and the fall of $\sigma_\gamma(E)$ with increasing E approximately as $1/E^{2.5}$ when E is larger than the binding energy of the atomic shell that absorbs the photon, this term asymptotically converges to the pure Rutherford $1/E^2$ cross-section. For hard collisions the other terms become negligible and the total cross-section converges to the Rutherford one, as expected. But

the $1/E^2$ factor before the integral of the fourth Rutherford term is only an approximate representation of the energy dependence of the free scattering. A more precise form could be (see, for example, [19,33,37,38])

$$R(E) = \frac{1}{E^2}\left(1 - \frac{\beta^2 E}{E_{\max}}\right) \tag{5}$$

where $E_{\max}$ is the maximum allowed transferred energy

$$E_{\max} = 2\frac{M^2 m_e c^2 \beta^2}{(M^2 + m_e^2 + 2\gamma M m_e)(1-\beta^2)} \tag{6}$$

where M is the mass of the incident particle and $\gamma = 1/\sqrt{1-\beta^2}$. In Eq. (5) we neglect the spin of the particle, which has negligible effect. For electrons and positrons the original $1/E^2$ factor is a good approximation provided we impose a maximal energy transfer equal to half the energy of the incident particle. In addition, we remark that in the case of dense media an additional factor $1/|\varepsilon|^2$ should be included in terms 1 and 3 of Eq. (1). In gases it is close to unity and can be skipped.

2.2. Separation of atomic shells

Let us assume that each portion of the transferred energy is absorbed by a single atomic shell. Equation (1) can then be reinterpreted as a sum of partial cross-sections responsible for absorptions by particular shells. The separation can be approximate for our purposes, but we want to keep the total value precise. Since Eq. (1) depends on $\sigma_\gamma(E)$, we should start, of course, from a similar reinterpretation of $\sigma_\gamma(E)$, which is well justified. Replacing $\sigma_\gamma(E)$ in (1) by a corresponding sum of cross-sections representing all shells and atoms in a mixture one obtains straightforward separation of three terms in (1). (Of course, the dielectric permeability (2) is computed with the total $\sigma_\gamma(E)$.) The term number 2 in Eq. (1) does not contain $\sigma_\gamma(E)$ as a factor, and cannot be separated directly. It is related to Cherenkov radiation, which is produced effectively by the total media, rather than by single atoms. Since our concern is the ionization, we will neglect this term under the ionization threshold $I_{\min}$. However this term does not completely vanish above threshold (where it cannot be interpreted as Cherenkov light). Fortunately this term is very little numerically, and we can distribute it uniformly among the shells, providing that the total (1) is not affected.

So $\sigma_\gamma(E)$ in expression (1) has to be replaced by a value corresponding to the electrons of a particular atom and shell $f(n_a)\sigma(E, n_a, n_s)$, where $f(n_a)$ is the fraction of atoms of a given sort in the gas, $\sum_{n_a} f(n_a) = 1$, n_a denotes the atom and n_s the shell. In addition, for the first and for the third term (which we are going to unify into one) only the ionization part of the photoabsorption cross-section, i.e. only the photoionization cross-section, which we will denote as $\sigma_{\gamma i}$, should be taken into account. To provide the correct asymptotic behavior the last term should contain the absorption cross-section, not the ionization one. However, it should not make a contribution below the ionization threshold of the atom $I(n_a)$, where discrete excitation levels in $\sigma_\gamma(E)$ could appear [17]. The possibility of excitation above the ionization threshold can be neglected.

Thus, the excitations will not be taken into account directly at the calculation of the energy-transfer cross-section (although they will influence it indirectly through dielectric permeability in which they are taken into account). This is an approximation, since excitation of one atom can sometimes cause ionization of another one having smaller ionization potential (the Jesse effect [17,39]).

As a result, the probability of ionization of a certain atom n_a and shell n_s, normalized per one atom of the medium, is given by the cross-section:

$$\begin{aligned}\frac{\mathrm{d}\sigma_i(E, n_a, n_s)}{\mathrm{d}E} = {} & \frac{\alpha}{\beta^2\pi} \\ & \times \left(\frac{f(n_a)\sigma_{\gamma i}(E, n_a, n_s)}{E|\varepsilon|^2} \ln\left(\frac{2m_e c^2 \beta^2}{E\sqrt{(1-\beta^2\varepsilon_1)^2 + \beta^4 \varepsilon_2^2}} \right) \right. \\ & \left. + H(E - I_{\min}) \frac{f(n_a)\sigma_{\gamma i}(E, n_a, n_s)}{\bar{\sigma}_\gamma(E)} \frac{1}{N\hbar c} \right. \\ & \left. \times \left(\beta^2 - \frac{\varepsilon_1}{|\varepsilon|^2} \right) \theta + H(E - I(n_a)) R(E) \right)\end{aligned}$$

$$\times \int_0^E f(n_a)\sigma_\gamma(E_1, n_a, n_s)\,\mathrm{d}E_1 \Bigg). \qquad (7)$$

Here $\bar{\sigma}_\gamma(E)$ is the mean photoabsorption cross-section $\sum_{n_a,n_s} f(n_a)\sigma_\gamma(E, n_a, n_s)$, $H(x) = 1$ for $x > 0$ and $H(x) = 0$ otherwise. The random sampling according to Eq. (7) allows one to choose atoms, shells, and energy values for the Monte Carlo simulation of primary interactions.

2.3. Atomic data

The photoabsorption data were taken from Refs. [40–44]. When only the total cross-section was given (as in Ref. [40]), the shells were separated phenomenologically by taking into account typical energy dependence of the partial cross-sections (see Section 2.1). Atomic shell energies are taken from Ref. [45]. We currently use only the atomic cross-sections even when the atoms constitute a molecule. This is well justified for internal shells and a first-order approximation for valent shells. But when the atomic ionization potentials are less than the molecular ones, the cross-sections of the corresponding atomic valent shells are adjusted by simple shift of the cross-sections toward larger energies by the value of difference between the molecular and atomic ionization potentials, thus providing the agreement between the left edges of photoionization cross-sections and the molecular ionization potentials. The few electron-volt shifts of individual shells have no impact on the mean energy losses, but noticeably affect the number of energy transfers (of small energies) and lead to good reproduction of available experimental data. However, using this simple approach means the neglect of effects such as neutral dissociation, molecular excitation, etc. Some molecular ionization potentials are taken from Ref. [46].

2.4. Emission of secondary particles

The energy transferred from the incident particle is assumed to be absorbed by a single atomic electron, which leaves the atom. By analogy with the photoeffect this electron is called the photoelectron. It is expected to carry an energy equal to the transferred energy minus the binding energy of this electron before collision. Note that the photoeffect itself is also simulated by the program, since among the relaxation products there are the fluorescent photons and they need to be traced. In the case of absorption of a real photon, the photoelectron is emitted in the direction of motion of the photon. In the case of collision with charged particles the distribution of directions of the photoelectron emittance over the azimuthal angle ϕ is isotropic. The polar angle is well approximated by the angle of momentum transfer at the collision with a free electron, in which the given energy is transferred [16]. For slow transfers at collisions with fast charged particles, i.e. for most of the collisions, this angle is very close to 90°.

After the emission of the photoelectron the atom is left in an excited state with a vacancy in the ionized shell and relaxes via the emission of the fluorescent photons as well as autoionization (Auger) electrons. The program can model any user-determined sequence of transitions, but by default it executes the following simplified standard sequence (corresponding to some experimental data [17]). The vacancy at any given shell is first filled from the shell with the next principal quantum number, and the first Auger electron is emitted from the next shell as well. Then the two vacancies remaining in the next shell are filled from the outermost shell and another two Auger electrons are emitted from the outermost shell. The energy of each Auger electron is given by the binding energy of the filled shell minus twice the binding energy of the freed shell. The probability of fluorescence is usually small, but fluorescence is simulated instead of the above-described autoionization cascade if it occurs in the Monte Carlo process. The set of data on fluorescence is supplied by the program `mucal`, Ref. [47]. In the end the atom is left with ionized outermost shells and is not considered anymore.

2.5. Absorption of δ-electrons

The total length of δ-electron way can be roughly estimated by integration of a formula for

continuous energy losses, applied in small steps. But this length will be much longer than the practical range of δ-electron, which is measured in experiments (approximately two times longer). The δ-electron is strongly scattered by atoms and never flies by a straight line. The scatterings can also be simulated together with the continuous energy losses, if one simulates the deflection of the trajectory after each step by an angle computed according to the elastic scattering cross-sections. This gives results consistent with the practical range, though the possibility of multiplication of δ-electrons is not taken into account. The δ-electron can then be assumed to leave only low-energy conduction electrons on its way. The mean work per pair production w and the Fano factor F allow us to generate the random number of conduction electrons deposited at each step with correct mean and fluctuations. But this will be a real number, whereas in order to generate the conduction electrons in a computer simulation we need an integer one. Rounding real to integer would case uncontrolled change of the dispersion and the average. This can be avoided if the residual from rounding is remembered and taken into account at the next step. The integer number of electrons can then be uniformly distributed along the current step. There is also a way to simulate a slightly non-uniform space distribution of conduction electrons along the step (this is closer to reality), if we assume that the energy losses on the step are distributed uniformly, but the energy spent for deposition of each next conduction electron E_c fluctuates according to some appropriate distribution. These fluctuations should contribute to fluctuations of the final number of deposited electrons, which means the effective rise of F. It is very convenient that by adjusting the parameters of the E_c-distribution we can totally reproduce the required value of F (as well as w for large energies) automatically, without any other random additions.

Let us assume that we are at the beginning of modeling the first step of the continuous energy losses. We choose a small enough straight step Δx and compute by a phenomenological formula the energy loss ΔE of the δ-electron at this step. Then we choose the energy E_c necessary for the next conduction electron by random sampling. We also introduce an auxiliary variable ΔE_r with an initial value ΔE. If $E_c \leqslant \Delta E_r$, a new conduction electron is deposited at a point spaced from the previous one at $E_c/(\Delta E/\Delta x)$, E_c is subtracted from ΔE_r, and the process is repeated until the next E_c is more than ΔE_r. The difference $E_c - \Delta E_r$ becomes the first E_c for the next step. If the energy of δ-electron is exhausted, the last difference remains unused, but the δ-electron itself becomes the last conduction electron.

Phenomenological considerations and numerical tests show that an appropriate shape of the distribution for E_c could be, for example, a uniform distribution from $w/2$ to w and shaped as $(w/E_c)^4$ from w to $3.064w$ (and zero outside these limits). This gives the average w and the dispersion corresponding to $F = 0.174\ldots$. It is convenient to generate a random number E_{cs} with some "standard" value w_s (in HEED $w_s = 30.0$ eV and $F_s = 0.174$) and to pass to the actual supplied by the user values of w and F by formulas: $E_c = kE_{cs} + a$, $k = w/w_s \cdot \sqrt{F/F_s}$, $a = w(1 - \sqrt{F/F_s})$.

The unused energy residual (the last difference $E_c - \Delta E_r$) leads to rise of the effective value of w for little incident energies. This increasing occurs in reality as well: it is observed in experiments [39] and obtained in detailed calculations [17,39], although the data are very fragmentary and often of doubtful dependability. According to review [39] many calculations show approximately the same behavior:

$$W(E_e) = \frac{W_a}{1 - V/E_e} \tag{8}$$

where E_e is the initial energy of the incident electron, W is the total mean work per pair production (up to absorption of the incident particle and all secondaries), W_a is the asymptotic W value for high E_e (similarly w_a will be asymptotic w, $w_a = W_a$), and V is some constant having the dimension of energy. Qualitatively, it is tempting to assign $V = I_{min}$ or approximately $w_a/2$, since this suppresses the ionization automatically when E_e approaches I_{min}. It is interesting that the precise calculations, as well as the simple phenomenological algorithm described above, give

similar values for V. The algorithm gives $V \approx 10.7$ for argon. This is however less than appears in a Monte Carlo simulation in Ref. [17], $V \approx 15.7$. In addition, this "default" V does not provide a good agreement between the energy loss distributions and the ionization distributions in the energy units (the number of conduction electrons multiplied by w_a) for high energy particles in gaseous layers. Thus, unless an additional correction is introduced, w_a for high energy particles is not reproduced well enough by the model. The behavior of total W Eq. (8) is approximately reproduced by the algorithm described above with the following energy dependence for differential w:

$$w(E_e) = \frac{w_a}{1-(V/E_e)^2}. \tag{9}$$

The rise of W obtained in Ref. [17] is approximately reproduced by putting $V = w_a/2$ in Eq. (9). This also gives a good agreement between the energy loss and ionization distributions.

For calculation of the continuous energy loss ΔE of δ-electron in medium in the current version of the program we use the same algorithm as in the subroutine GDRELE of the program GEANT3 [33] with some modifications for energies less than 1 keV. The mean works per pair production used in this paper are given in Table 1. The value of this parameter for mixtures, modeled in this work, was calculated by averaging with taking into account molecular charges:

$$\bar{w} = \sum_m [f(n_m)Z(n_m)w(n_m)] \Big/ \sum_m [f(n_m)Z(n_m)] \tag{10}$$

where n_m is the index of the molecule, $f(n_m)$ the relative number of molecules of given sort in the mixture, and $w(n_m)$ the work for pure gas from Table 1. F is assumed to be 0.19 for any gas [39,49,50]. The elastic scattering cross-sections of electrons on atoms are taken from Ref. [51]. The small angle scatterings are too numerous to be modeled directly, but their total effect can be described by very simple methods [52,53]. The larger angle scatterings can be modeled by ordinary random sampling. The division into soft and hard collisions and their separated treatment

Table 1
The ionization potentials I_{min} and the work per pair production w (asymptotic) for some gases

Gas	I_{min}[eV][a]	w[eV][b]	Gas	I_{min}[eV][a]	w[eV][b]
He	24.59	41.3	CO_2	13.79	33.0
Ne	21.56	35.4	CF_4	16.23	34.3[c]
Ar	15.76	26.4	CH_4	12.71	27.3
Kr	14.00	24.4	C_2H_2	11.41	25.8
Xe	12.13	22.1	C_2H_4	10.51	25.8
H_2	15.43	36.5	C_2H_6	11.50	25.0
N_2	15.58	34.8	C_3H_8	11.07	24.0
O_2	12.08	30.8	i-C_4H_{10}	10.55	23.4
N_2O	12.89	32.6	$C_3H_8O_2$	10.00	22.1[d]

The data are taken from the following sources:
[a]from Refs. [45,46].
[b]from Ref. [39] unless otherwise indicated.
[c]from Ref. [48].
[d]$w(iC_4H_{10}) \cdot I_{min}(C_3H_8O_2)/I_{min}(iC_4H_{10})$.

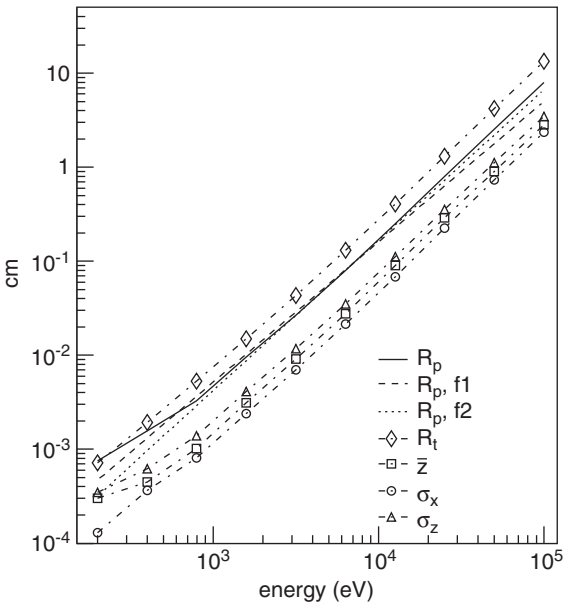

Fig. 1. The practical range R_p of the electrons in argon calculated by HEED (solid line) and two empirical formulas (dashed and dotted lines). Also shown are the total length of way of electrons R_t by HEED (rhombuses), the mean z-position $\bar{z}$ (if z is the initial direction of movement) of the "centers of gravity" of the ionization clouds (boxes) and its fluctuations (RMS) along the z-axis σ_z (triangles) and x-axis σ_x (circles).

by a "condensed simulation scheme" and by conventional random sampling respectively is frequently referred to as Berger's class II procedures [35,36,52,54].

The ionization effect of δ-electrons simulated by the total Monte Carlo algorithm appears to be in a good agreement with experiments. For example, Fig. 1 shows the practical ranges calculated by the program and by the phenomenological formulas [55], whose parameters were fitted by many experiments:

$$R = 3.872 \times 10^{-3} \times A/Z \times E^{1.492} \quad \text{for } 0.37\,\text{keV} < \text{E} < 10\,\text{keV} \tag{11}$$

$$R = 6.97 \times 10^{-3} \times E^{1.6} \text{ for } 10\,\text{keV} < \text{E} < 50\,\text{keV}. \tag{12}$$

Here the practical range R is measured in mg/cm^2 and the electron initial energy E in keV. HEED reproduces both formulas quite well in the limits of their applicability. Only at very small energies, less than 500 eV, does the practical range by HEED slightly exceed the first formula, although it is valid till 370 eV. Although at energies smaller than 1 keV the trajectory simulations by HEED are less precise due to some extrapolations, which needed to be introduced, the results are nevertheless quite reasonable even for these energies.

The same figure shows other interesting characteristics of electron trajectories which can be extracted from calculations by HEED. We see that many parameters of electron trajectories in material are proportional to the practical range, including the position of the "center of gravity" of the ionization and its fluctuations. This agrees with conclusions from Refs. [55,56].[2]

3. Comparisons with experiments

3.1. Numbers of primary clusters

The integral over E of Eq. (7), multiplied by the electron density, gives the number of energy transfers per unit length traveled by the incident particle. This number is practically identical to the number of primary ionization clusters measured in many experiments and frequently referred to as the specific primary ionization. This parameter is practically important because it determines the time resolution of various triggers (see, for instance, Refs. [7,24]) and also used for many other purposes [20]. Fig. 2(a) shows that the results obtained by HEED are in reasonable agreement with experimental data.

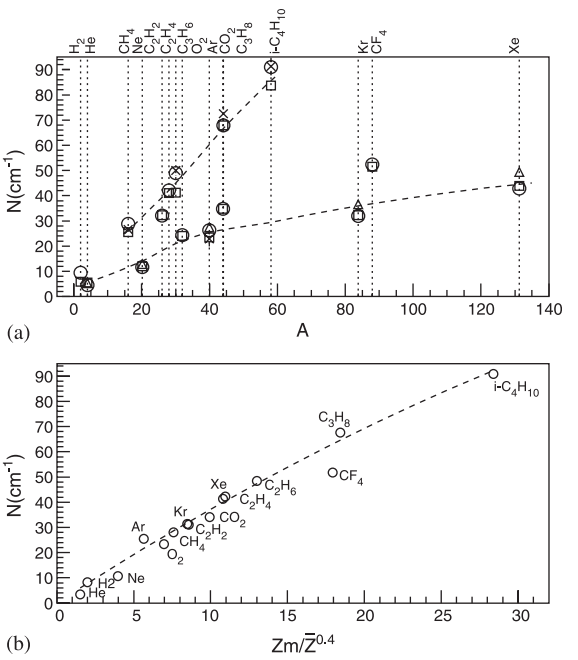

Fig. 2. The number of primary clusters for minimum-ionizing particles for various gases at NTP according to calculations by HEED (circles) and a number of measurements: Ref. [57] (squares), the average of numbers from Ref. [18] and seven other works quoted in Table 5 of Ref. [18] (stars), and Ref. [58] (triangles). (a) shows the dependency on the atomic or molecular weight. (b) shows the data of HEED only as function of $Z_m/\bar{Z}^{0.4}$. In (a) the dashed lines are drawn by hand to guide the eye. In (b) the dashed line represents fit to the given points except CF_4: $3.996x - 0.025x^2$ ($x = Z_m/\bar{Z}^{0.4}$).

This figure also shows that the number of primary clusters is not a good function of the molecular weight or the gas density (for different gases at the normal temperature and pressure). Only most hydrocarbons are on a straight line,

[2]However, the ratio between $\bar{z}$, σ_z, and σ_x plotted in the figure depends on the type of gas. Heavier gases are noted to give smaller $\bar{z}$ and larger σ_x due to stronger elastic scattering.

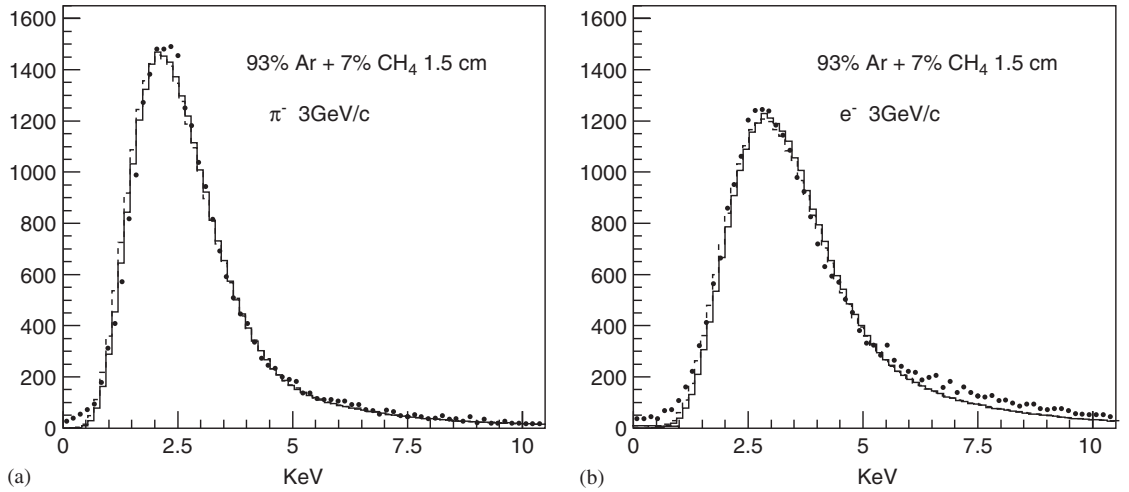

Fig. 3. The experimental (points) and theoretical "ionization loss" distributions expressed in energy units. Histograms drawn by solid lines are obtained by the PAIR model, dashed lines (they are practically coincide with solid ones) are by the PAI model.

which is obviously a manifestation of the similar atomic structure. All non-hydrocarbons lie below this line. There are two explanations for this: the first is the non-proportionality of Z_m (the total molecular charge) and A_m (the total molecular weight) and non-proportionality of the electron density to the mass density, and the second is that with increase of Z and A more and more electrons reside in deeper energy levels and, owing to the $1/E \ln E$ factor in the first term of Eq. (7), they interact less frequently with the incident particle. If we want to see all the points at one line, first of all we have to replace A_m by Z_m at the axis definition but that would not be enough.[3] To characterize the "deep" of electron levels in molecule we can use the mean atomic charge $\bar{Z} = \sum(f(n_a) * Z(n_a))/\sum f(n_a)$ of constituent atoms. Obviously, the higher $\bar{Z}$, the smaller the number of primary clusters at the same other conditions. $\bar{Z}$ should therefore appear in denominator, but its power is not derived from general considerations and can just be fitted. The appropriate value (at which all the points fall along a single curve) appear to be about 0.4, see Fig. 2(b). Only CF_4 does not fall on this line, perhaps due to the unusually large ionization potential of this molecule, 16.23 eV [59], which is noticeably higher than that of its neighbours, 11.5 eV for C_2H_6 and 11.07 eV for C_3H_8 [46]. It is also remarkable that out of the three gases not belonging to either category in Fig. 2(a): C_2H_2, CO_2, and CF_4, two are successfully described by the common law in Fig. 2(b). Obviously, one can use this correlation for making estimations for other gases.

3.2. The amount of ionization

3.2.1. The amplitude spectra in proportional chambers

There are a few published amplitude spectra of signals in proportional chambers, in which the amplitude scale is given in the units of energy, and the calibration is performed by registering X-rays with known energy, see Figs. 3 and 4. In fact, these spectra show with which probability the incident charged particle produces a signal equivalent to a signal produced by a photon of a certain energy. Our model gives us the number of electron–ion pairs. But if w is known, the equivalent photon energy and the number of pairs can be converted to each other. We plot the graphs in the energy units. Besides the simulations by PAIR, we plot

[3] Walenta [60] observed a correlation between the numbers of clusters for some gases and a variable whose significant part is $Z_m/I_{\min}$. But hydrocarbons do not correlate with it.

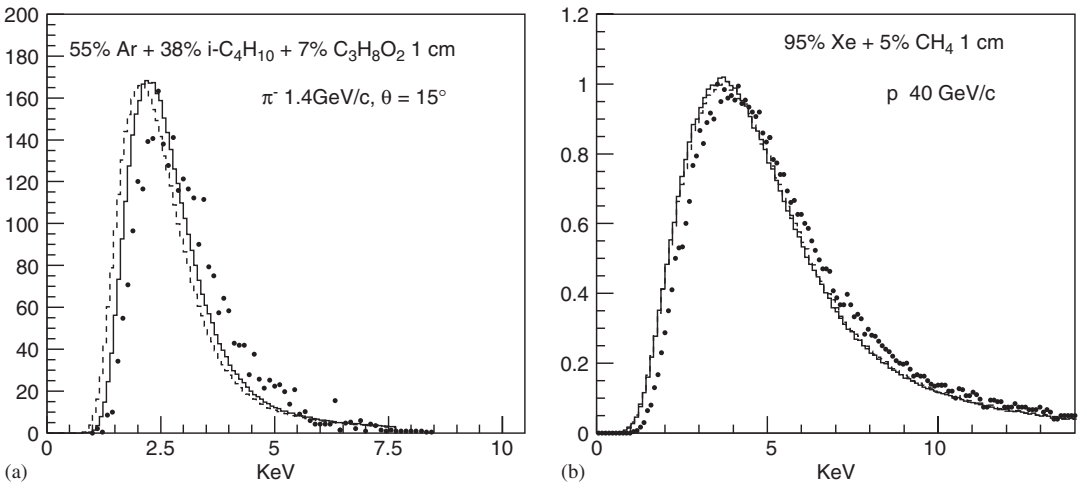

Fig. 4. The same as in the previous figure but for experiments [65] (a) and [64] (b).

the simulations made by the simple PAI model summing up the transferred energy obtained by Eq.(7). In this procedure the parameter w is not used (except for some very little correction of device resolution, see below) and its numerical value does not matter. However, comparing the PAI curve with the experimental spectrum we assume that w for incident fast charged particle is equal to W for the photon. At the calculations by the PAI model with relaxation, described in the given work, the value of w is used to obtain the ionization effect from δ-electrons. The comparison with the experimental curve requires the use of w for backward conversion from the total amount of ionization to the equivalent photon energy. If the whole model is consistent (including the asymptotic values and energy dependence of w), the average of PAIR and PAI spectra should coincide.

Unfortunately, the calibration by X-rays is not always precise due to triggering problems. The work [61] claims 20% precision of calibration only. The precision of the measurements presented in Fig. 4 is unknown.

The width of the photopeak allows one to estimate the chamber resolution. At the registration of the fast charged particles the resolution has little effect, but nevertheless slightly influences on the width of the registered distribution. The statistical precision, with which the ionization is measured in proportional chambers, is approximately proportional to the square root of the signal amplitude (see, for example, Ref. [62]). Therefore for the purpose of simulations it is sufficient to determine the resolution for any one amount of ionization and to assume that it is scaled accordingly for the others. We have to subtract from the width of the photopeak the fraction related to the Fano factor. Simulating the event by PAIR we obtain the number of conduction electrons, convert it to the energy loss (multiplying it by w), determine the device resolution for this energy, and obtain the corresponding fluctuation of the measured signal by random sampling from Gaussian distribution. Simulating the event by PAI we obtain the energy loss and the number of energy transfers. Then we determine the device resolution for this energy loss. The difference between the energy loss divided by w and the number of energy transfers gives us roughly the amount of secondary ionization, which has to fluctuate according to the Fano factor. We compute the corresponding dispersion, add it to the dispersion of the device resolution and finally generate the corresponding fluctuation of the measured signal by random sampling. The

resolution of the proportional chamber studied in the work [61] can be taken from the photopeak in the previous work of the same authors [63] and it is about 0.36 keV at the energy 2.5 keV. The resolution of the experiment [64] is not known, but the modeling with the same resolution, as for the paper [61], leads to agreement with the experiment. At the modeling of the experiment [65] the resolution of 5% from the amplitude quoted in the paper was used.

Spectra in Fig. 3 are obtained during a test of a chamber in the transition radiation detector with removed radiator. Spectrum in Fig. 4(b) is measured in the transition radiation detector with radiator, but with very little value γ of incident particle, at which the transition radiation is negligible [66]. The simulations are performed for 293 K and 1 atm (760 Torr) except for Fig. 4(a), where the pressure is 730 Torr [65].

From the results of modeling, shown in Figs. 3 and 4, one can see that the both approaches to modeling, PAI and PAIR, give close results and well agree with experiments. The PAI and PAIR distributions are practically identical to each other for argon and xenon-based mixtures (Figs. 3 and 4(b)) and differ slightly only in the case of large admixture of hydrocarbons (Fig. 4 (a)) . In the latter case there is also some subtle difference between both curves and experiment. The modeling of this distribution by the PAI model is also performed in the work [65] with small statistics but with apparently better agreement with the experiment than that of the PAI model by HEED. One or both spectra from the work [61] were also modeled by PAI in works [15,16,18,22,31,38,67] with demonstration of reasonable agreement between the models and the experiment.[4]

[4]Although the agreement between different calculations is not quite perfect, since they sometimes deviate from the experiment in different directions. This can be explained by slightly different equations, by different input atomic data, and by the various strong simplifications of the basic equations, such as the replacement of continuous photoionization cross-section by a few discrete lines. In this work we follow the precise Eq. (7) and compute it using a very fine logarithmic energy mesh.

3.2.2. The spectra of the truncated means in the multi-layer detectors

Multi-layer ionization detectors are used for particle identification. The convenient characteristic of ionization effect is a truncated mean of measured amplitudes. From n amplitudes a_k, $k = 1, \ldots, n$, measured for a given track, one chooses a certain number of the least amplitudes (let us denote their fraction by p and the corresponding integer number by n_p) and calculate their average, which we denote $\langle a \rangle_n^p$. The truncated mean obviously fluctuates from event to event. The distributions of the truncated means $\langle a \rangle_{64}^{40\%}$ (the mean of 25 least amplitudes chosen from 64 measurements) measured in the work [68] for various gases and for protons, pions and electrons with momenta 15 GeV/c are given in Fig. 5. While the proton with momentum 15 GeV/c stays in the vicinity of the ionization minimum, the electron with the same momentum is at the Fermi plateau. At the modeling of these spectra two free parameters, the ratio channel/(amount of ionization) and the resolution at some amount of ionization, were adjusted for the best description of the proton peak and used for the modeling of the pion and electron peaks. In Fig. 5 one can see that this simulation reproduces both peaks for all checked gases. Some small deviations were obtained only for krypton and for hydrocarbons. The program directly modeled 64 adjacent gaseous volumes without any material borders between them and without wires, generated straight incident track through them, and allowed all secondary particles (δ-electrons and photons) to pass freely from one layer to another (such penetration has however little influence on results).

3.2.3. The averaged truncated mean as a function of velocity

The dependence of the average value $\overline{\langle a \rangle_{128}^{40\%}}$ in 6-cm argon layers on $\beta\gamma$ was measured in Ref. [62] and was later analyzed in papers [15–18,22,31]. Refs. [15,18] give only the total height of the Fermi plateau, which is approximately 1.60 according to their graphs. The $\beta\gamma$-dependencies from the other works are reproduced in Fig. 6 together with the results obtained by HEED.

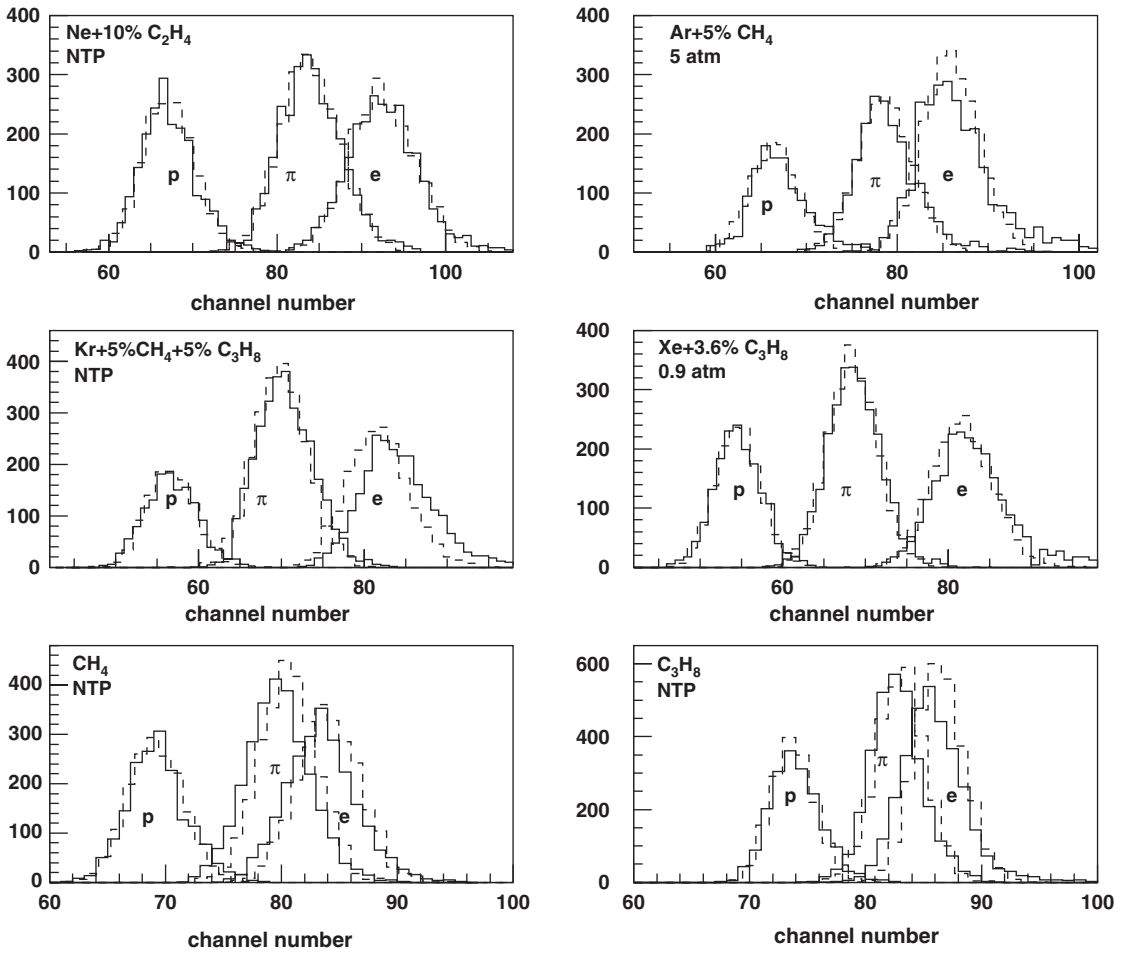

Fig. 5. The distributions of $\langle a \rangle_{64}^{40\%}$ for layers of 4 cm width for protons, pions, and electrons with momentum 15 GeV/c. Experimental data [68] are given by solid curves. Dashed lines are simulation by HEED according to PAIR model.

The modeling of this experiment by HEED included simulation of 128 adjacent gaseous volumes without material between them, without wires, and with penetration of secondaries to neighboring layers. The device resolution taken into account in simulation was 0.82 keV (the Fano factor subtracted) for the absorbed energy 10.0 keV, the atmospheric conditions were 293 K and 730 Torr. The statistical resolution was automatically plotted for each point, but it is not seen in the figure, since it is less than the point size. The plotted curve is obtained with protons as incident particles. The results for electrons are practically identical.

The general behavior of all curves is the same (except a strange left tail of the curve from Ref. [17], which is likely a result of some technical confusion). However, there are some small but noticeable discrepancies between all theoretical and experimental results.

The discrepancies between theoretical curves are explained by the remark (see footnote 4 on previous page) and by the sensitivity of the results to the input atomic data, mainly to the photo-ionization cross-section. All available tables of cross-sections are incomplete and differ from each other. For example, while HEED with the cross-section for argon compiled by Henke et al. [40]

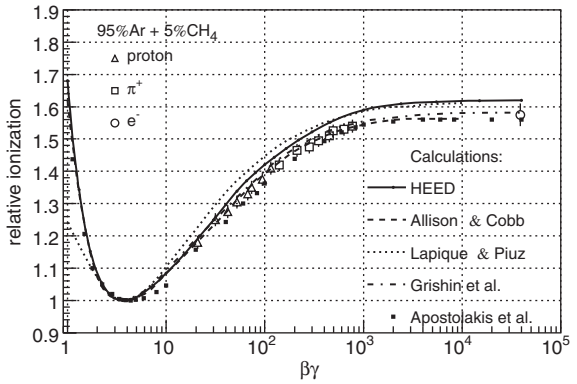

Fig. 6. The relative ionization according to experiment [62] and simulations: by HEED (this work, truncated mean by PAIR), and by Allison and Cobb [16] (the most probable ionization by PAI for 4.5 cm of pure argon), by Lapique and Piuz [17] (truncated mean by PAIR for pure argon), by Grishin et al. [31] (truncated mean by PAI), and by Apostolakis [22] (the most probable ionization by PAI).

gives the total rise of the truncated mean equal to 1.62, the same program with almost identical cross-section for argon given earlier by Marr and West [42] gives approximately 1.56 (the same result as in Refs. [16,22]). Although the table of Marr and West can be declined since it does not reproduce the experiment described in the next section, on the basis of the calculating experience with this and other cross-sections we can assume that the systematic uncertainty of the Fermi plateau height theoretical predictions can be up to 5–10% of the relative height with respect to the minimum (that is 5–10% of 0.6 in the case of argon).

Walenta [69] has obtained that the truncated mean and the most probable ionization behave similarly. This is confirmed by HEED qualitatively, but quantitatively the height of the Fermi plateau determined by the most probable ionization is approximately by 0.015–0.02 lower than that determined by the truncated mean for the conditions of this experiment. Therefore the estimates of the full rise from Refs. [15,16,18,22] have to be increased by 0.02 for correct comparison with the truncated means, since these papers give rise in terms of the most probable ionization.

The work of Lapique and Piuz [17] was the only paper, in which the shells of argon were separated (it was not explained how it was done) and the relaxation cascades were simulated by a very detailed way. But δ-electron elastic scattering and presence of a small admixture of methane were not taken into account. The obtained curve is higher than the experimental points. It is also higher than the HEED curve in the intermediate region where the ionization rises, but it saturates at the same level with HEED.

The linearity of the detection system in the experiment is checked very well, but the experimental data lack reliable normalization. The ionization in the minimum was not measured due to the absence of the low energy beam. The data were normalized by rather an indirect way with involving other less precise measurements and Landau–Sternheimer theory predictions for low velocities [70–72].[5] This means that the only important fact for comparison with PAI(R) models is the relative positions of these experimental points. Put another way, we have to renormalize the data by the model calculations. The most convincing results are obtained at normalization by several first experimental points with the lowest $\beta\gamma$ (several points are taken in order to suppress the statistical straggling of the experimental points). For example, using all proton points we obtain the normalization factor 1.0218 and good coincidence between the other points and the curve, Fig. 7. Thus, the results of HEED agree with this experiment. The results of other calculations also agree more or less. It is also interesting that the curve computed by HEED almost coincides with the Landau–Sternheimer theory [74–78] at low $\beta\gamma$ up to $\beta\gamma \approx 80$. This makes their normalization factors almost identical. Fig. 7 then indicates that the Landau–Sternheimer theory disagrees with this experiment despite of the data renormalization.

Looking carefully at Figs. 6 and 7 one can notice that the transition from the relativistic raise to the Fermi plateau according to HEED is not gradual, but has some structure (though this effect

[5] It is also interesting that the next work of the same group [73] gives higher relativistic rise, which agrees with our calculations. But we will not consider it here, since it does not have the minimal point as well.

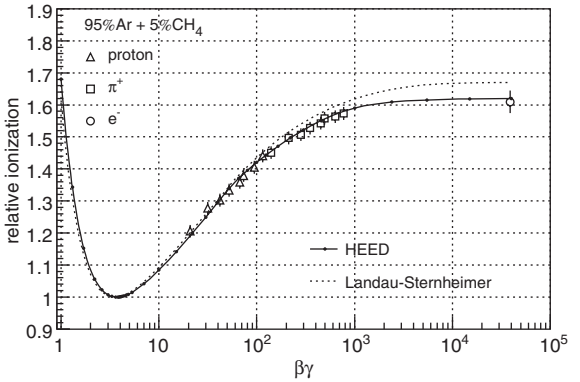

Fig. 7. The simulations of experiment [62] by HEED (truncated means by PAIR) and by the Landau–Sternheimer theory (the most probable ionization) compared with the normalized experimental data.

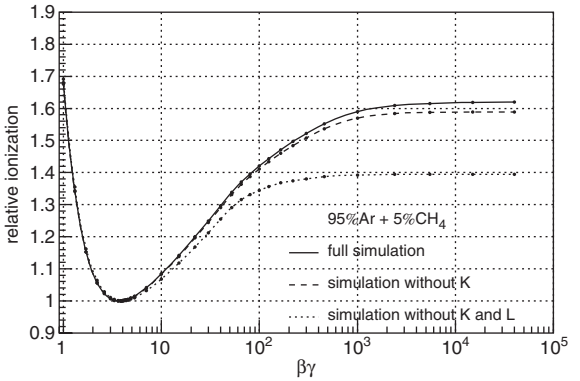

Fig. 8. The simulations of experiment [62] by HEED (truncated means by PAIR) by the full program (the solid line), and also without taking into account interactions with K-shell of argon (the dashed line), or without interactions with K- and L-shells of argon (the dotted line).

is not seen clearly in the graphs of the other authors). After the nearly straight portion (with slight acceleration of rise) in the region of $\beta\gamma \approx 20$–50, the curve exhibits sudden "local" deflection at $\beta\gamma \approx 70$ and continues to rise with noticeably smaller and nearly constant speed in the interval of $\beta\gamma \approx 90$–250. As can be seen in Fig. 8, the physical explanation of this effect is a sudden and fast saturation of the interactions with the M-shell. Fig. 8 convinces that the usual notion about the gradual transition from rise to saturation *is not justified*. This transition can have a structure corresponding to the atomic shells. However, the magnitude of this effect depends on the details of the calculation procedure and on the cross-sections used.

3.2.4. *The most probable ionization as a function of velocity*

The behavior of the most probable ionization was directly measured in an experiment [69]. The advantage on this experiment, if compared with one from the previous section, is the availability of measurements nearly in the minimum of ionization, while the disadvantage is smaller statistical precision of the measurements. The detector was also tested with X-rays and one may assume the absence of the device saturation effects at the atmospheric pressure (this is not the case for higher pressure). The device resolution taken into account in simulation was 0.39 keV for the absorbed energy 5.96 keV, the conditions were 293 K and 760 Torr. The most probable ionization was determined by Monte Carlo spectra by several methods, which gave consistent results. The most precise methods are fitting upper parts of the peaks by certain asymmetric bell-shaped functions.

The comparison of the calculations with the experiment is shown in Fig. 9. We can see a good agreement. In particular, for argon the experimental value of the full relativistic rise is 1.59 ± 0.04 (with the uncertainty taking into account the uncertainties of the last and of the minimal point). The theoretical value obtained with normalization at the same value of $\beta\gamma = 3.2$, at which the measurements are performed (Fig. 9 is drawn by this way), is 1.618 ± 0.004 (statistical resolution). That is the calculated value is inside one standard deviation from the experimental value. It needs however to remark, that the theoretical minimum occurs at slightly different $\beta\gamma$, (approximately at 3.6) and is less than the value at $\beta\gamma = 3.2$ by a factor of approximately 1.006. If we renormalize the results, we obtain 1.60 ± 0.04 for the experiment and 1.628 ± 0.004 for theory. We can see again two almost straight segments at the curve for argon to the left and to the right side from $\beta\gamma \approx 70$, the structure effect discussed in the

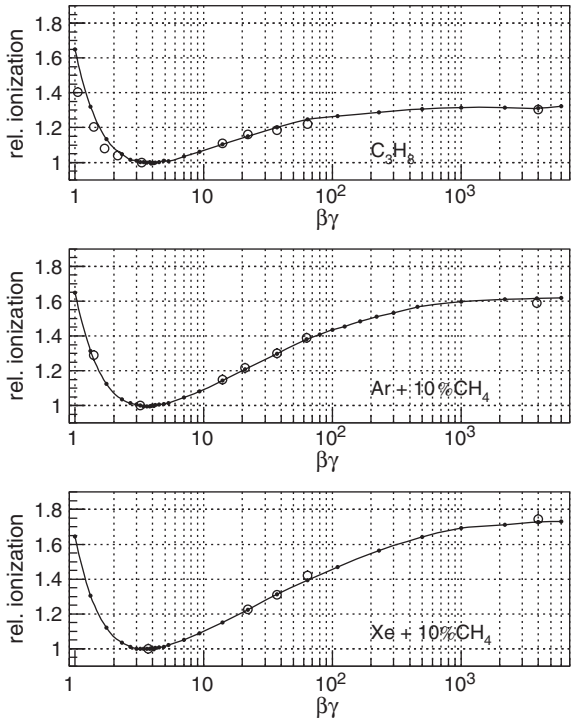

Fig. 9. The dependency of the most probable ionization on the particle velocity according to experiment [69] (circles) and modeling by HEED according to PAIR (points connected by solid lines) in three different gases at normal temperature and pressure in the layer of 2.3 cm width. The statistical errors do not exceed the marker widths.

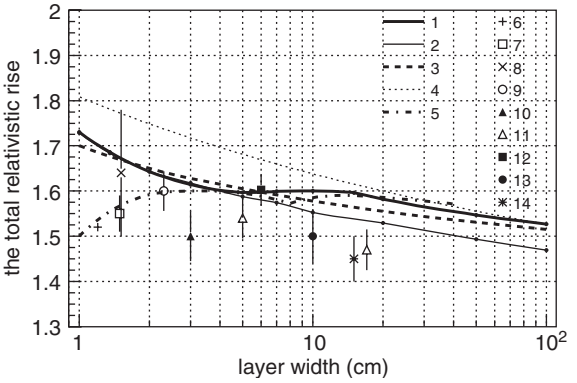

Fig. 10. The total relativistic rise of the most probable ionization in argon at NTP as a function of the layer width. Curves: 1—the calculation by HEED by the PAIR model for $Ar + 5\%CH_4$; 2—the same but without the K-shell of argon; 3—the calculation from the work [18] by the PAI model; 4—the Landau–Sternheimer theory for $Ar + 5\%CH_4$; 5—the corrected Landau–Sternheimer theory [79]. The points are the experimental data from the following works: 6—[80] ($Ar + 5\%C_3H_8$ with taking into account the correction factor 1.05 for right minimum and maximum, the resolution is unknown); 7—[82] ($Ar + 20\%CO_2$); 8—[61] ($Ar + 7\%CH_4$); 9—[69] ($Ar + 10\%CH_4$); 10—[70] ($Ar + 5\%CH_4$); 11—[81] ($Ar + 5\%CH_4$); 12—[62] ($\langle a \rangle_{128}^{40\%}$ for $Ar + 5\%CH_4$ with normalization by the PAIR model, see text and Fig. 7, here the height and the resolution of the last normalized experimental point is plotted); 13—[83] (Ar); 14—[84] ($Ar + 7\%CH_4$).

previous section. Unfortunately there is no experimental points in the region of the second segment, but the first segment seems to be perfectly confirmed by the experiment. Similar structure is seen at the curve calculated for C_3H_8, but it is not seen for xenon. The external atomic shells of Xenon are closer to each other by binding energies, and their influence is not distinguished by this way.

3.2.5. The relativistic rise of the most probable ionization as a function of the layer width

The ratio of the most probable ionization at the Fermi plateau to that in the minimum can be plotted as a function of the layer width. We will repeat here the figure for argon taken from Ref. [18] (an earlier version with a fewer experimental points is in Ref. [15]) with our additions and corrections based on analysis of the original papers, Fig. 10. Besides the experimental data and calculations by HEED this figure shows the PAI calculations from Refs. [15,18], the Landau–Sternheimer curve (our calculation by [74–78] agrees with a curve from Ref. [18]), and a curve calculated in Ref. [79] by a corrected Landau–Sternheimer model. As can be seen, all these curves differ from each other and from the data. It is well known about the difference between the Landau–Sternheimer theory and the PAI theory. The difference between the empirical approach of Ref. [79] and both the PAI theory and the Landau–Sternheimer curve is rather unexpected, since this purely empirical method is derived from them and it should be close at least to one of them. The coincidence of this curve with two experimental points number 6 and 7, which are not

described by the PAI(R) models, is not important, since the point number 6 does not have error bars at all (the error is not determined in the paper and it is probably large), and the point number 7 has strong systematic uncertainties described later. Therefore this empirical approach does not seem to be well justified. However, this curve was first demonstrating structure effects in this dependence (which were perhaps missed in more complicated and time consuming calculations by PAI in Refs. [15,18]). A sharp minimum at 8 cm width was explained in Ref. [79] by the absorption edge of an internal atomic shell. Calculations by HEED with the current set of cross-sections do not confirm the existence of such sharp minimum, but reveal rather a pronounced plateau at layer widths 5–10 cm (formally there might be a minimum, but very shallow and broad: 1.597 ± 0.002 at 5 cm against 1.600 ± 0.003 at 10 cm; the other cross-sections can give deeper minimum, but it is similarly broad and appears at the same place: 5 cm against the maximum at 10 cm). The plateau is caused by the interactions with the K-shell of argon. This is proved by a special calculation in which the interactions with the K-shell where ignored and the plateau disappeared, Fig. 10. The plotted curves represent PAIR, but the results ofPAI are practically identical. The device resolution was not taken into account here, the atmospheric conditions were 293 K and 760 Torr.

Among the experimental points only three agree with the PAI(R) calculations: points number 8 [61], 9 [69], and 12 [62]. The reader can easily recognize that these points represent the familiar experiments which are already considered in more detail in the previous sections (see Figs. 3, 7, and 9). The point number 11 at 5 cm width almost agrees with the PAI(R) calculations as well. All the other points lie below the PAIR curve farther than one standard deviation from it. However a detailed analysis of the papers reveals that although corresponding experiments (it concerns also Refs. [61,62]) were useful in many other respects, they did not give exhaustive information for determination of the full relativistic rise. There were shortcomings such as the absence of check of linearity (or comments about it in the papers) [70,80,81], not sufficient maximal X-ray energy at calibration [84], an indefinite minimal or maximal point (which leads to some theory-based corrections or extrapolations) [61,62,70,80,82], an indefinite resolution of particle identification or measurement of its $\beta\gamma$ [81,83], high cross-talks between channels [82], significant admixture of different gas [82]. Therefore the only fully credible point is point number 9 [69] (however, some tiny normalization had to be made even in this case, see Section 3.2.4) and this point agrees with the PAI(R) theory (both with HEED and with Ref. [15,18]).

In addition we remark that at the widths smaller than 4 cm the peak position is determined by the interactions with L- and M-shells. As first pointed out by Allison [85], below 1 cm in argon the spectra become irregular with effects of single shells being seen. For argon the energies of shells L1, L2, and L3 are 248, 251, and 326 eV, which is compatible with the width of ionization distribution produced by the interactions with the M-shell for layers narrower than 1 cm. For such layers the probability of interactions with L-shells is not too high. Therefore the events where such interactions do not occur at all can form one peak, and the events with one or a few such interactions form the second peak. At certain conditions these peaks can acquire equal height, thus forming two equally "most probable" ionizations, as in Fig. 11. This can happen at low or high $\beta\gamma$, e.g., at the Fermi plateau. In the last case it can be said that the Fermi plateau is splitted (if determined by the most probable ionization, of course) and two Fermi plateaus are instead formed at different positions, see 11(a). Another case, when a similar effect appears in the minimum of ionization, is shown in Fig. 11(b).

3.3. Space fluctuations of ionization

A good opportunity to test how well the model predicts the space fluctuations of initial ionization is provided by measurements of the ultimate space resolution of position sensitive proportional chambers irradiated by X-rays. At certain conditions the electron ranges are dominate contributors in the position line width. Modeling such experiments by HEED involves and, therefore, allows

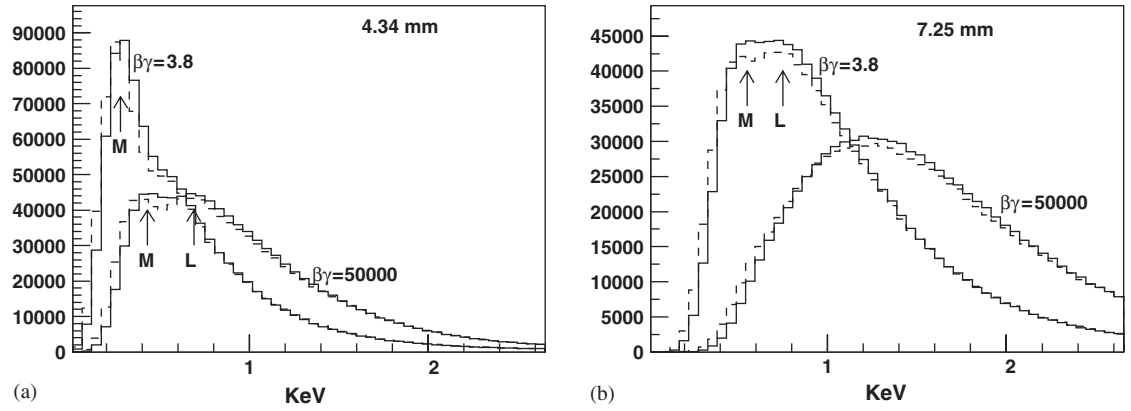

Fig. 11. The ionization spectra (distributions of 1 million events) by PAIR (solid lines) and energy losses by PAI (dashed lines) for argon+5% methane mixture at NTP for the layer width 4.34 mm (a) and 7.25 mm (b) in the ionization minimum and on the Fermi plateau. The effects of the argon M- and L-shells are clearly seen. In (a) they cause the splitting of the Fermi plateau, if it is determined by the most probable ionization. In (b) similar effect is exhibited by the most probable ionization at ionization minimum.

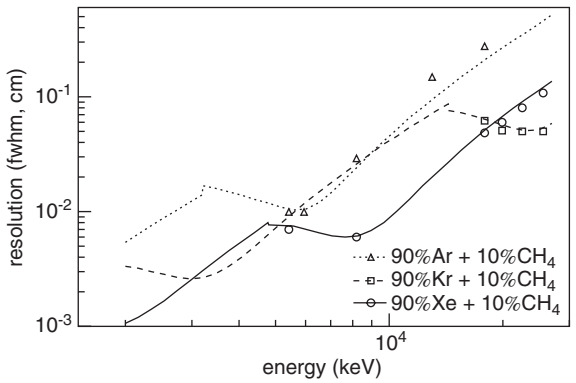

Fig. 12. The resolution (fwhm) of the position sensitive proportional chamber with several different gases at NTP irradiated by X-rays. The experiment [56] and the calculation by HEED.

one to test the simulation of the photoabsorption process, the atomic relaxation cascades, the absorption of secondaries, and the formation of conduction electrons (but the cross-section (7) is not tested by this way). The measurements from [56] and our simulation of this experiment are presented in Fig. 12. In the simulation a photon of a certain energy was emitted along the z-axis into a wide gas volume. If it was absorbed, the x or y-position of the "center of gravity" of conduction electrons produced was registered as the measured position. Only the "photopeak" events were selected by an appropriate amplitude cut (as in the experiment). The width at half-height of the corresponding distribution was plotted in Fig. 12. One can see that the simulation reproduces well the experimental data except two points for argon measured at relatively high energy. The agreement of these two points with the simulation is slightly poorer (due to unknown reason), but still acceptable. The pronounced structure effects seen at these curves are discussed in Refs. [55,56].

In order to check the modeling of space fluctuations occurring in a gas in the case of the incident fast charged particle (which includes Eq.(7)), we can compare the simulations with the experimental data that were obtained during testing of the prototypes of the cathode strip chambers (CSC) designed for the end-cap muon system of the CMS experiment at CERN [24]. The measured strip charges allow one to determine the position of the "center of gravity" of ionization produced by the incident particle, see Figs. 13. The bell-shaped form of the central part is well described by a simple model developed in Ref. [24], in which the fluctuations occur due to the noise in the registered strip charges. The magnitude of noise is determined by the fluctuations of

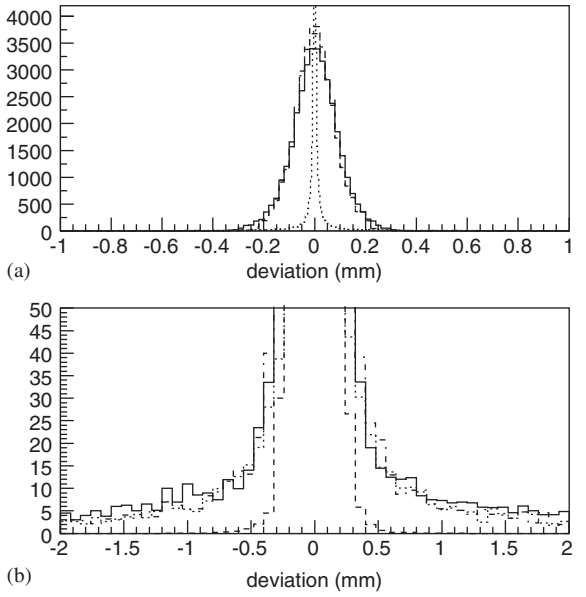

Fig. 13. The space resolution (in two different scales) of a cathode strip chamber prototype ($30\%Ar + 40\%CO_2 + 30\%CF_4$ at NTP) measured in experiment [24] (solid lines), modeled taking into account the strip noise [24] (dashed lines), displacements of initial ionization by HEED (dotted lines), and the space resolution modeled by a combined method taking into account the strip noise and displacements (dash–dotted lines).

the pedestals. In Fig. 13(a) there are, however, small tails that are more visible in the increased scale in Fig. 13(b). Obviously the tails are not explained by this simple model. In Ref. [24] these tails were reproduced by some artificial tuning of the simulation with adding extra hits (additional incident tracks) to a fraction of events. As can be seen, the simulation of single tracks by PAIR with relaxation and absorption of secondaries allows us to reproduce these tails almost totally. This indicates once more that the theoretical model and the computer program work correctly.

4. Conclusions

The PAI model reproduces quite well the numbers of primary clusters, the amplitude spectra and the relativistic dependencies of ionization in gaseous detectors. The separation of atomic shells, the simulation of relaxation cascades and absorption of secondary particles, which can be called the PAIR model, allows one to describe also the space distribution of ionization. The results of modeling agree well with experimental data. The models can be used for research and development of gaseous detectors of fast charged particles.

Acknowledgements

The author would like to thank for support of this work, stimulating discussions, and help A.A. Vorobyov, R. Veenhof, P. Nevski, O.E. Prokofiev, and M.B. Trzhaskovskaya.

References

[1] R. Veenhof, GARFIELD, A Drift Chamber Simulation Program, CERN, 1994, CERN program library, entry W5050, http://cern.ch/garfield, Nucl. Instr. and Meth. A 419 (1998) 726.
[2] I.B. Smirnov, CERN Comput. Newslett. 226 (1996) 13.
[3] A.I. Akhiezer, N.F. Shulga, High Energy Electrodynamics in Matter, Nauka, Moscow, 1993 (in Russian).
[4] W. Riegler, Limits to drift chamber resolution. Dissertation, Techn. University of Vienna, November 1997.
[5] W. Riegler, et al., Nucl. Instr. and Meth. A 443 (2000) 156.
[6] W. Riegler, Nucl. Instr. and Meth. A 494 (2002) 173.
[7] W. Riegler, C. Lippmann, R. Veenhof, Nucl. Instr. and Meth. A 500 (2003) 144.
[8] M.N. Mazziotta, Comput. Phys. Commun. 132 (2000) 110.
[9] G. Velichko, Performance Simulation of Cathode Strip Chamber Prototype P1. CMS Note 2000/022.
[10] V. Nikulin, AliHEED, the ROOT wrapper for HEED, http://cern.ch/nikulin.
[11] M.M. Aggarwal, et al., Nucl. Instr. and Meth. A 488 (2002) 131.
[12] U. Fano, Ann. Rev. Nucl. Sci. 13 (1963) 1.
[13] V.A. Chechin, L.P. Kotenko, G.I. Merson, V.C. Yermilova, Nucl. Instr. and Meth. 98 (1972) 577.
[14] V.A. Chechin, V.C. Ermilova, Nucl. Instr. and Meth. 136 (1976) 551.
[15] V.C. Ermilova, L.P. Kotenko, G.I. Merzon, Nucl. Instr. and Meth. 145 (1977) 555.
[16] W.W.M. Allison, J.H. Cobb, Ann. Rev. Nucl. Part. Sci. 30 (1980) 253.
[17] F. Lapique, F. Piuz, Nucl. Instr. and Meth. 175 (1980) 297.
[18] V.C. Asoskov, V.M. Grishin, V.K. Ermilova, L.P. Kotenko, G.I. Merson, V.A. Chechin, Ionization Effects

in Real Detectors of Relativistic Charged Particles, Trans. Lebedev Phys. Inst. 140 (1982) 1 (in Russian).
[19] H. Bichsel, Rev. Mod. Phys. 60 (1988) 663.
[20] U.A. Budagov, G.I. Merson, B. Sitar, V.A. Chechin, Ionization Measurement in High Energy Physics, Energoatomizdat, Moscow, 1988 (in Russian) (Revised and enlarged English edition, B. Sitar, G.I. Merson, V.A. Chechin, U.A. Budagov, Ionization Measurement in High Energy Physics, Springer, Berlin, etc., 1993).
[21] V.M. Grishin, V.K. Ermilova, S.K. Kotelnikov, Nucl. Instr. and Meth. A 307 (1991) 273.
[22] J. Apostolakis, et al., Nucl. Instr. and Meth. A 453 (2000) 597.
[23] P.R. Collins, Nucl. Phys. B (Proc. Suppl.) 117 (2003) 391.
[24] M.M. Baarmand, et al., Nucl. Instr. and Meth. A 402 (1998) 36.
[25] J. Sempau, et al., Nucl. Instr. and Meth. B 132 (1997) 377;
J. Sempau, et al., Nucl. Instr. and Meth. B 207 (2003) 107.
[26] M. Brigida, et al., Nucl. Instr. and Meth. A 533 (2004) 322.
[27] H. Bichsel, R.P. Saxon, Phys. Rev. A 11 (1975) 1287.
[28] R. Talman, Nucl. Instr. and Meth. 159 (1979) 189.
[29] V.A. Soloshenko, Energy Losses by Charged Particles, ITEF, preprint-114, 1980 (in Russian).
[30] S.P. Ahlen, Rev. Mod. Phys. 52 (1980) 121.
[31] V.M. Grishin, V.K. Ermilova, S.K. Kotelnikov, Nucl. Instr. and Meth. A 309 (1991) 476.
[32] D.H. Wilkinson, Nucl. Instr. and Meth. A 401 (1997) 263.
[33] R. Brun, et al., GEANT3: User's Guide, CERN, Data Handling Division.
[34] GEANT4, http://cern.ch/wwwasd/geant4.
[35] EGS4, http://ccwww.kek.jp/kek/rad/egs4/egs.html.
[36] EGS4nrc, http://www.irs.inms.nrc.ca/inms/irs/EGS4/get_egs4.html.
[37] E.A. Uehling, Ann. Rev. Nucl. Sci. 4 (1954) 315.
[38] I.B. Smirnov, Calculation of Ionization Loss Fluctuations of Fast Heavy Charged Particles, PNPI, preprint-1758 (1991) (in Russian).
[39] Average Energy Required to produce an Ion Pair, ICRU Report 31, 1979.
[40] B.L. Henke, E.M. Gullikson, J.C. Davis, At. Data Nucl. Data Tables 54(2) (1993) X-Ray WWW Server of the Uppsala University, Sweden, http://xray.uu.se/.
[41] E.L. Kosarev, E.P. Podoliak, Opt. & Spectrosk 56 (1984) 643 (in Russian).
[42] G.V. Marr, J.B. West, At. Data Nucl. Data Tables 18 (1976) 497.
[43] D.A. Verner, D.G. Yakovlev, I.M. Band, M.B. Trzhaskovskaya, At. Data Nucl. Data Tables 55 (1993) 233.
[44] M.B. Trzhaskovskaya, Private communication, 1995.
[45] G. Williams, Electron Binding Energies, X-Ray WWW Server of the Uppsala University, Sweden, http://xray.uu.se/.
[46] V.N. Kondratiev, Energies of Chemical Connections, Potentials of Ionization, Affinity to Electron, The Reference Book, Moscow 1974 (in Russian).
[47] P. Bandyopadhyay, The Program for Generation of Fluorescence Yield, X-Ray WWW Server of the Uppsala University, Sweden, http://xray.uu.se/.
[48] G.F. Reiking, L.G. Christophorou, S.R. Hunter, J. Appl. Phys. 60 (1986) 499.
[49] G.D. Alkhazov, A.P. Komar, A.A. Vorob'ev, Nucl. Instr. and Meth. 48 (1967) 1.
[50] G.D. Alkhazov, Zh. Tekhn.Fiz 41 (1972) 1949 (Sov. Phys. Tech. Phys. 16 (1972) 1540).
[51] M.E. Riley, C.J. MacCallum, F. Biggs, At. Data Nucl. Data Tables 15 (1975) 443;
M.E. Riley, C.J. MacCallum, F. Biggs, At. Data Nucl. Data Tables 16 (1975) 379.
[52] M.J. Berger, Meth. Comput. Phys. 1 (1963) 135.
[53] B. Rossi, High-Energy Particles, Prentice-Hall, Englewood Cliffs, NJ, 1952.
[54] F. Salvat, Rad. Phys. Chem. 53 (1998) 247.
[55] L.P. Lapina, A.G. Sergeev, A.I. Smirnov, Position Resolution of Proportional Chamber for X-rays Detection, PNPI, Preprint-2022 (1994) (in Russian).
[56] J. Fisher, V. Radeka, G.C. Smith, Nucl. Instr. and Meth. A 252 (1986) 239.
[57] F.F. Rieke, W. Prepejchal, Phys. Rev. A 6 (1972) 1507.
[58] A. Pansky, G. Malamud, A. Breskin, R. Chechik, Nucl. Instr. and Meth. A 323 (1992) 294.
[59] L.G. Christophorou, et al., Nucl. Instr. and Meth. A 309 (1991) 160.
[60] A.H. Walenta, et al., Physica Scripta 23 (1981) 354.
[61] F. Harris, et al., Nucl. Instr. and Meth. 107 (1973) 413.
[62] I. Lehraus, R. Matthewson, W. Tejessy, M. Aderholz, Nucl. Instr. and Meth. 153 (1978) 347.
[63] S. Parker, et al., Nucl. Instr. and Meth. 97 (1971) 181.
[64] V. Commichau, et al., Nucl. Instr. and Meth. 176 (1980) 325.
[65] H. Frehse, et al., Nucl. Instr. and Meth. 156 (1978) 87.
[66] B. Dolgoshein, Nucl. Instr. and Meth. A 326 (1993) 434.
[67] J.H. Cobb, W.W.M. Allison, J.H. Bunch, Nucl. Instr. and Meth. 133 (1976) 315.
[68] I. Lehraus, R. Matthewson, W. Tejessy, Nucl. Instr. and Meth. 200 (1982) 199.
[69] A.H. Walenta, et al., Nucl. Instr. and Meth. 161 (1979) 45.
[70] D. Jeanne, et al., Nucl. Instr. and Meth. 111 (1973) 287.
[71] M. Aderholz, P. Lazeyras, I. Lehraus, R. Matthewson, W. Tejessy, Nucl. Instr. and Meth. 118 (1974) 419.
[72] I. Lehraus, Private communication, 2003.
[73] I. Lehraus, R. Matthewson, W. Tejessy, Nucl. Instr. and Meth. 196 (1982) 361.
[74] L. Landau, J. Physics (USSR) 8 (1944) 201.
[75] H.D. Maccabee, D.G. Papworth, Phys. Lett. 30A (1969) 241.

[76] R.M. Sternheimer, R.F. Peierls, Phys. Rev. B 3 (1971) 3681.
[77] R.M. Sternheimer, M.J. Berger, S.M. Seltzer, At. Data Nucl. Data Tables 30 (1984) 261.
[78] K.S. Kölgib, B. Schorr, Comput. Phys. Commun. 31 (1984) 97.
[79] V.M. Grishin, G.I. Merson, Nucl. Instr. and Meth. A 274 (1989) 551.
[80] Z. Dimcovski, et al., Nucl. Instr. and Meth. 94 (1971) 151.
[81] E.A. Kopot, et al., J. Exp. Theor. Phys. 70 (1976) 387.
[82] W.W.M. Allison, et al., Nucl. Instr. and Meth. 133 (1976) 325.
[83] J.K. Parry, H.D. Rathgeber, J.L. Rouse, Proc. Phys. Soc. A 66 (1953) 541.
[84] P.V. Ramana Murthy, et al., Nucl. Instr. and Meth. 63 (1968) 77.
[85] W.W.M. Allison, Physica Scripta 23 (1981) 348.